Cell Biochem Biophys (2018) 76:3–17
DOI 10.1007/s12013-017-0811-8

REVIEW ARTICLE

EPR Characterization of Dinitrosyl Iron Complexes with Thiol-Containing Ligands as an Approach to Their Identification in Biological Objects: An Overview

Anatoly F. Vanin[1,2]

Received: 28 January 2017 / Accepted: 10 June 2017 / Published online: 19 July 2017

Abstract The overview demonstrates how the use of only one physico-chemical approach, viz., the electron paramagnetic resonance method, allowed detection and identification of dinitrosyl iron complexes with thiol-containing ligands in various animal and bacterial cells. These complexes are formed in biological objects in the paramagnetic (electron paramagnetic resonance-active) mononuclear and diamagnetic (electron paramagnetic resonance-silent) binuclear forms and control the activity of nitrogen monoxide, one of the most universal regulators of metabolic processes in the organism. The analysis of electronic and spatial structures of dinitrosyl iron complex sheds additional light on the mechanism whereby dinitrosyl iron complex with thiol-containing ligands function in human and animal cells as donors of nitrogen monoxide and its ionized form, viz., nitrosonium ions (NO^+).

Keywords Dinitrosyl iron complexes · Nitrogen monoxide · Thiol-containing ligands · Living objects · EPR spectroscopy

Abbreviations

B- or M-DNIC	Binuclear or mononuclear dinitrosyl iron complexes
DETC	Diethyldithiocarbamate
EPR	Electron paramagnetic resonance
HFS	Hyperfine structure
MNIC	Mononitrosyl iron complex

✉ Anatoly F. Vanin
vanin@polymer.chph.ras.ru

[1] N. N. Semenov Institute of Chemical Physics, Russian Academy of Sciences, Moscow, Russia

[2] Institute for Regenerative Medicine, I. M. Sechenov First Moscow State Medical University, Moscow, Russia

In 1963, Dr Robert Nalbandyan and I undertook an electron paramagnetic resonance (EPR) study in order to investigate the ability of baker's yeast (Saccharomyces cerevisiae) cells to generate free radicals. Incidentally, we discovered in their EPR spectra a weak EPR signal with a top at $g = 2.04$ corresponding to a downfield shift of 50 Gauss from the EPR signal of free radicals ($g = 2.0$) [1].

Further experiments showed that this peak corresponded to the low-field component of the EPR signal: its shape and position in the magnetic field are shown in Fig. 1 [2]. The amplitude of the EPR signal recorded in dried yeast cells at 30 °C decreased with the increase in the registration temperature from 150 to 360–370 K in full conformity with the Curie-Weiss law for paramagnetic compounds. At higher temperatures, this EPR signal declined gradually to the point of irreversible disappearance and was not accompanied by significant changes in the signal shape (Fig. 1).

From these data, we concluded that the low- and high-field components of the EPR signal corresponded to two different parts of the same signal with the following characteristics of the g-factor: $g_\perp = 2.04$, $g_\parallel = 2.014$, $g_{aver.} = 2.03$ (Fig. 1). Based on the mean value of the g-factor, we defined this signal as a 2.03 signal. As this EPR signal represented the first derivative of the EPR absorption curve and contained five turns characteristic of EPR signals of polycrystalline paramagnetic centers with an axial spatial structure, we conjectured that it had only two values of the g-factor [2, 3].

The disappearance of the 2.03 signal from the EPR spectra of dried yeast cells at 80–90 °C prompted another

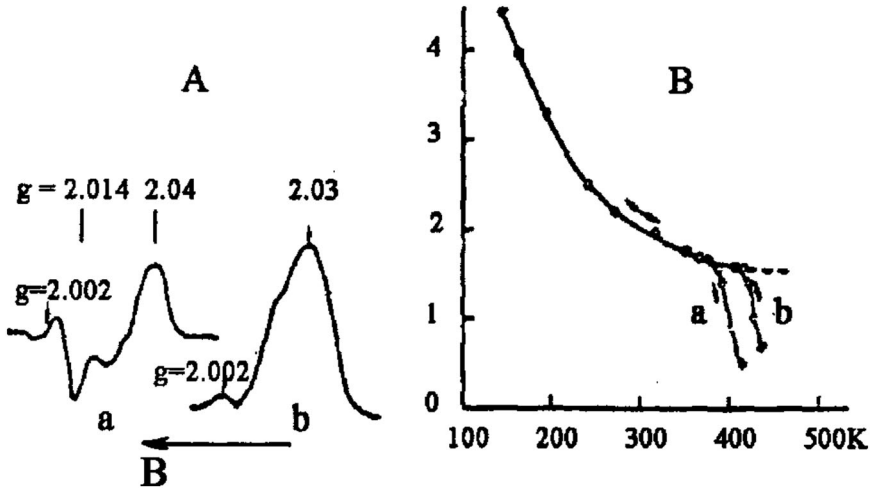

Fig. 1 **A** The first derivative of the EPR absorption curve recorded on an EPR radiospectrometer at ambient temperature **a** and the shape of the EPR absorption curve of the 2.03 signal (first integral of the curve a) **b**. **B** The temperature-dependent changes in the intensity of the 2.3 signal recorded in dried yeast cells placed into open **a** and hermetically sealed **b** ampoules [2]. Abscissa: registration temperature; ordinate: EPR signal intensity

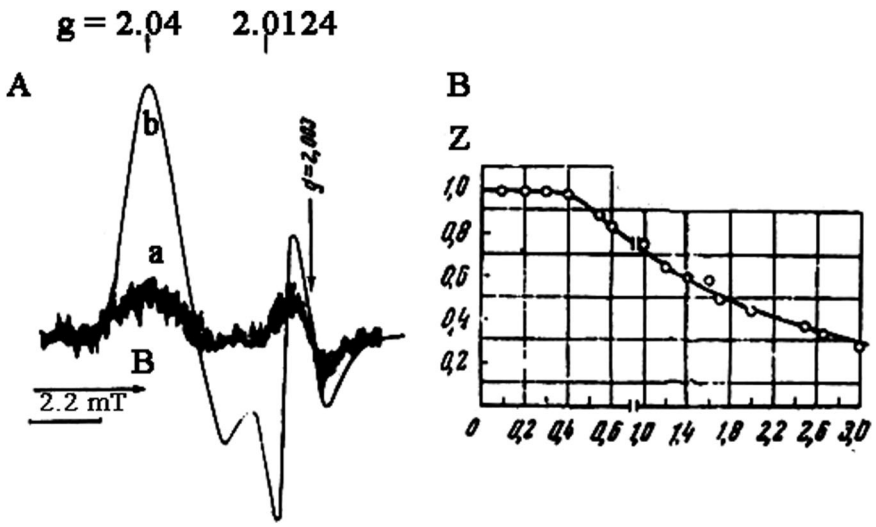

Fig. 2 **A** The 2.03 signal recorded in wet **a** and **b** dried yeast cells at ambient temperature. The EPR signal at $g = 2.0$ is due to free radicals localized in yeast cells. **B** Microwave saturation of the 2.03 signal in dried yeast cells at 77 K. Z—The intensity ratio between the 2.03 signal and the EPR signal of a Cu^{2+} salt unsaturable with the increase in the detector microwave power normalized to unity. Abscissa: microwave detector current (mA) [4]

conclusion, viz., the paramagnetic centers responsible for this signal were bound to proteins denaturing at this particular temperature. Supporting evidence was obtained in experiments where wet yeast samples generated a 2.03 signal at ambient temperature; its shape was identical to the shape of the 2.03 signals recorded in dried yeast cells at ambient temperature and in wet yeast samples at liquid nitrogen temperature (Fig. 2) [4].

This finding provided strong evidence for the protein origin of the paramagnetic centers responsible for the 2.03 signal. If in wet yeast cells the latter was generated by low-molecular centers, the increase in temperature from 77 K to ambient temperature would inevitably result in the averaging of the g-factor anisotropy by virtue of high mobility of paramagnetic centers at ambient temperature concomitant with a decrease in the 2.03 signal width.

Moreover, in our study the amplitude of the 2.03 signal in dried yeast cells decreased with the increase in the microwave power of the EPR radiospectrometer resonator due to microwave saturation of the 2.03 signal at 77 K (Fig. 2). The fact that this effect was unaccompanied by changes in the signal shape led us to hypothesize that the 2.03 signal was generated by the same paramagnetic centers and the widths of the spin packets in the 2.03 signal were significantly smaller than the width of the total signal, i.e., the broadening of the 2.03 signal might be qualified as non-homogenous.

The aforecited data first appeared in open press in 1964–1966 [1, 2, 4]. The significant deviation of the mean values of the g-factor of the 2.03 signal from the purely spin value (2.0024) described therein led us to conjecture that the paramagnetic centers responsible for this signal might contain "heavy" atoms. Judging from the principal values of their g-factor (2.04 and 2.014), these might be sulfur atoms [2, 4], since the ability of sulfur-containing paramagnetic centers to generate EPR signals in biological objects after

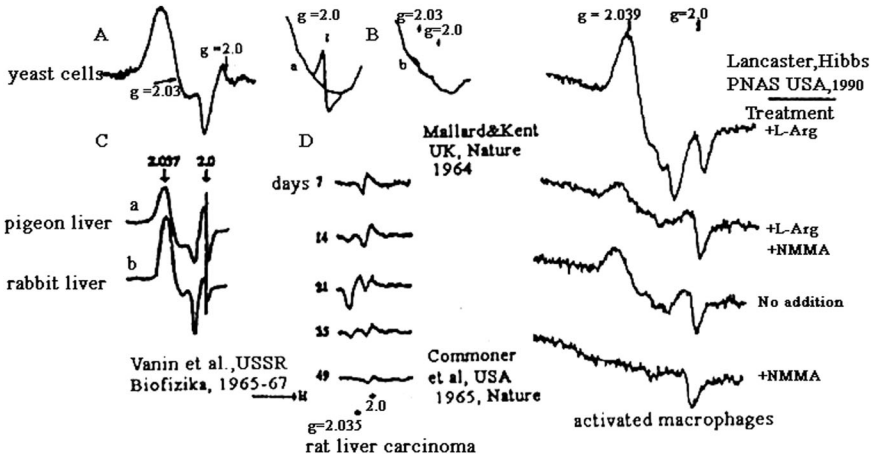

Fig. 3 The first records of the 2.03 signal in yeast cells **A** [1, 2] and rat liver carcinoma induced by butter yellow (*p*-dimethylaminoazobenzene) (**B** spectrum **b**) or **a** EPR spectra of normal liver [6]; pigeon and rabbit liver (**C**, spectra **a** and **b**), respectively [7]; **D**, livers from rats kept on a diet supplemented with butter yellow for 7, 14, 21, 35, and 45 days [5]. *Right* panel: The 2.03 signal recorded in 1990 in activated animal macrophages in the presence of L-arginine, L-arginine + NOS inhibitor *N*-methyl-L-arginine, in the absence of L-arginine and *N*-methyl-L-arginine and in the presence of *N*-methyl-L-arginine alone [8]

radiation treatment was already established by that time. The principal values of the g-tensor for such signals lie in the same range as those for the 2.03 signal. Treatment of yeast cells with thiol group blockers and complete disappearance of the 2.03 signal provided additional evidence in favor of this hypothesis [4].

Simultaneously and independently with our studies, a group of U.S. investigators led by Barry Commoner, who, parallel to the Soviet biophysicist Lev Blyumenfeld, was a pioneer in the use of the EPR method in biological research, published a paper [5] describing the detection of the 2.03 signal (or, more exactly, of its weak component, $g = 2.035$) in the EPR spectra of rat liver cells treated with hepatocarcinogenic agents (Fig. 3). This EPR signal was recorded in liver tissue 2 weeks after treatment of animals with hepatocarcinogenic reagents and gradually disappeared within a course of 1 month. In 1964, a 2.03 signal of even lower intensity was found in rat liver samples by the British investigators J. Mallard and M. Kent [6] (Fig. 3). However, further reports from these authors are absent in the literature, while Commoner and coworkers gave their discovery considerable attention: studies in this field continued most vigorously.

According to Commoner et al. [5], the discovery of the 2.03 signal in the livers of rats treated with hepatocarcinogenic agents should be regarded as a marker of malignant growth. However, our data [7] fully refuted this argument, since in our studies the 2.03 signal of high intensity was repeatedly recorded in rabbit and pigeon liver cells in the absence of malignant growth (Fig. 3).

Thirty years after the discovery of the ability of animal cells and tissues to produce nitrogen monoxide (NO), one of the most universal regulators of metabolic processes, NO was generated by NO-synthase isozymes from L-arginine. The 2.03 signal was recorded in various biological objects, mostly, in cultured cells able to synthesize NO by enzymatic route.

The 2.03 signal recorded by D. Lancaster and D. Hibbs in cultured activated macrophages (Fig. 3) [8] is an illustrative example. As can be seen, the inhibition of the inducible form of NO-synthase (iNOS) by *N*-methylarginine responsible for NO synthesis in these cells strongly attenuated the 2.03 signal, while the addition of the NO-synthase substrate (L-arginine) to the cultural medium enhanced it.

At this point, Commoner and coworkers and the members of our research team went different ways. The U.S. investigators used a standard biochemical approach to establish the nature of the paramagnetic centers responsible for the 2.03 signal in living objects, for example, fragmentation of tissues with subsequent determination of paramagnetic centers by the intensity of the 2.03 signal generated in different protein fractions [9]. These studies culminated in identification of the protein fraction able to generate a 2.03 signal of high intensity (as calculated per protein content in this fraction). However, the content of the paramagnetic centers in the fraction responsible for the 2.03 signal appeared to be as low as 5% of that in the original preparations. With this in mind, we chose a different, more venturesome approach, which consisted in a search for alternative paramagnetic compounds able to generate the 2.03 signal. And our ventures were crowned with success!

To our luck, in 1965 three U.S. chemists—C. McDonald, W. Phillips, and H. Mower published a paper in which they described the synthesis of EPR-active dinitrosyl iron complexes (DNIC) with various thiol-containing anionic ligands including L-cysteine [10]. However, the EPR signals of

these DNIC were recorded at ambient temperature and represented symmetric singlets with the half-widths of about 0.7 mT. For us, the most striking result of this study was full correspondence of g-factor characteristics of the singlet EPR signal of DNIC with cysteine to the mean EPR value, viz., 2.03.

This and the presence in DNIC of thiol groups of L-cysteine prompted the idea to examine whether the centers responsible for the 2.03 signal in biological objects represent DNIC with thiol-containing ligands. In our opinion, the lack of the difference between the widths of the EPR signals at both 77 K and ambient temperature (Fig. 2) might be attributed to the protein nature of the centers responsible for the 2.03 signal in biological objects: low mobility of the protein globule at ambient temperature could hardly be the reason for the averaging of the anisotropy of the g-factor as was the case with low-molecular DNIC, e.g., DNIC with cysteine ligands.

In order to obtain conclusive evidence for the hypothesis on the ability of protein-bound DNIC with thiol-containing ligands to generate the 2.03 signal, it seemed important to investigate possible coincidence of the EPR signal of low-molecular DNIC in frozen solutions and the 2.03 signal characteristic of biological objects. By some miracle, the EPR signals of frozen solutions of DNIC with L-cysteine recorded at liquid nitrogen temperature (77 K) showed a full coincidence between the 2.03 signals recorded in cells and tissues at ambient temperature and 77 K (Fig. 4d′ and Fig. 2A) [11]. In contrast, the shape of the EPR signals recorded in frozen solutions of DNIC with hydroxyl ions, water, or phosphate differed notably from that of the 2.03 signal (Fig. 4a′–c′).

The similarity of the 2.03 signals recorded in biological objects to the EPR signal of DNIC with L-cysteine used as a model compound enabled us to develop a directional approach to establishing the nature of the centers responsible for the 2.03 signal in living organisms. Treatment of these centers and model compounds able to react selectively with bivalent iron (iron chelators), thiol groups (heavy metals), and compounds endowed with the ability to substitute for thiol ligands (xanthogenate derivatives) initiated similar changes in the shape of the 2.03 signal, while the EPR signals of the model compounds changed in a similar way (Fig. 5) [7].

After treatment of yeast extracts with ethyl xanthogenate (Fig. 5d), the 2.03 signal converted into a EPR signal with a triplet hyperfine structure (HFS), evidently as a result of interaction of the unpaired electron with the nitrogen nucleus ^{14}N (nuclear spin $I = 1$) within the composition of mononitrosyl iron complexes (MNIC) with ethyl xanthogenate [7]. The changes in the shape of the 2.03 signal after treatment of yeast extracts with *p*-chloromercuribenzoate (PCMB) might be attributed to the substitution of thiol

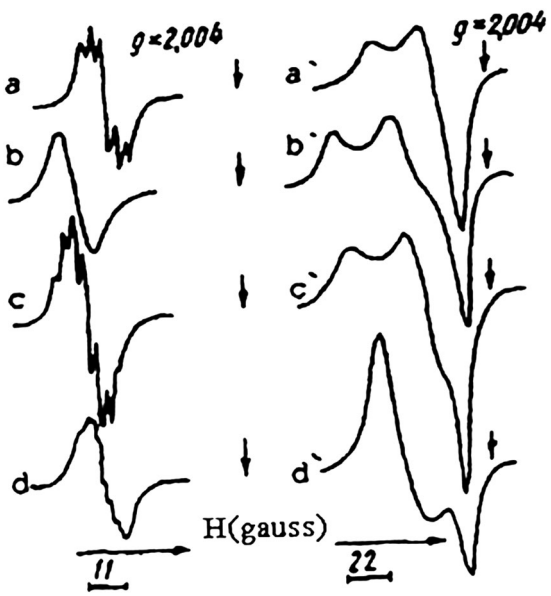

Fig. 4 The EPR spectra of DNIC with hydroxyl (pH 12.0) **a**, **a**′ water (pH 7.0) **b**, **b**′ phosphate **c**, **c**′, and cysteine **d**, **d**′ recorded at ambient temperature **a–d** or at 77 K **a**′**–d**′[11]

ligands for phosphate in DNIC after addition of PCMB to the yeast extracts (Fig. 5e). A similar substitution of thiol groups in DNIC for *o*-phenanthroline changed the shape of 2.03 and EPR signals of model compounds after treatment with iron chelators (Fig. 5b, h).

The results of these studies demonstrated full identity of the changes in the model compound and the paramagnetic centers responsible for the 2.03 signal in yeast cells. For simplicity sake, let us term them as 2.03 complexes. Again, I will call your attention to the fact that in biological objects these complexes exist predominantly in the form of protein-bound DNIC, while the role of thiol-containing ligands is played by protein-bound L-cysteine residues.

In animal tissues, the formation of 2.03 complexes was induced by treatment of animal tissues with gaseous NO, or by addition of the NO donor nitrite or particularly nitrite together with Fe-citrate to the drinking water of experimental animals (mice) [12, 13]. Simultaneous addition of sodium nitrite and ^{57}Fe-citrate instead of ^{56}Fe-citrate to the drinking diet of mice increased the width of the 2.03 signal recorded in mouse liver due to HFS from the ^{57}Fe nucleus (nuclear spin $I = 1/2$) (Fig. 6a, b). Similar changes were found in the EPR signal recorded in frozen solutions of DNIC with cysteine, the ^{56}Fe ($I = 0$) atom in which was substituted for ^{57}Fe (Fig. 6c, d). At ambient temperature, the EPR signal of the model compound was characterized by doublet hyperfine splitting instead of the singlet signal characteristic of the complex with ^{56}Fe (Fig. 6f, g) [14].

Identification of the nature of 2.3 complexes in biological objects (yeasts and animals tissues) as DNIC with thiol-

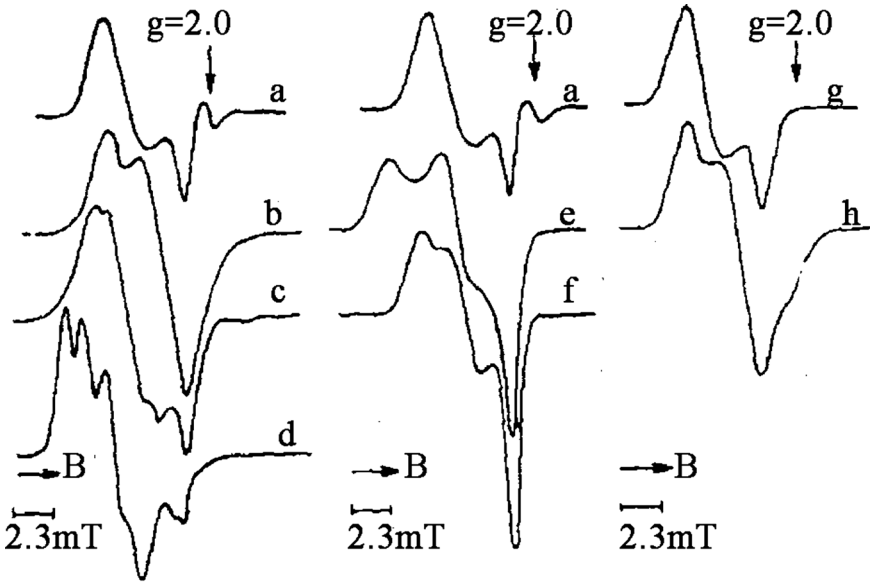

Fig. 5 The changes in the shapes of the EPR signals recorded in yeast cells **a** (*left* and *central* panels) and DNIC with cysteine **g** (*right* panel) treated with various reagents: *o*-phenanthroline **b**, **h**, dithiazone **c**, ethyl xanthogenate **d**, *p*-chloromercuribenzoate **e**, sodium dithionite **f**. The measurements were performed 5 min after addition of the reagents [7]

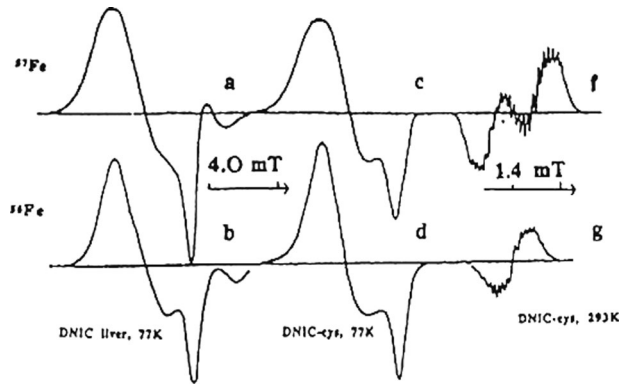

Fig. 6 The 2.03 signals recorded in the livers of mice kept on a drinking diet containing nitrite + Fe^{57} with citrate **a** or nitrite + Fe^{56} with citrate **b**. **c–g** The EPR signals of DNIC with cysteine containing Fe^{57} **c**, **f**, or Fe^{56}**d**, **g**. All EPR spectra were recorded at 77 K **a–d** or at ambient temperature **f**, **g** [14]

containing ligands and the EPR analysis of low-molecular DNIC with the same ligands shed additional light on their electron and spatial structures. Our first remarkable achievement was determination of the composition of the 2.03 complexes using HFS analysis of EPR spectra of low-molecular model compounds recorded at ambient temperature.

Figure 7a (*right* panel) depicts the 13-component HFS of the EPR signal of DNIC recorded at ambient temperature. The five-component HFS appearing in the EPR spectrum as a result of interaction of the unpaired electron with two atoms of ^{14}N ($I = 1$) unambiguously indicates the presence in DNIC of two equivalent nitrosyl (^{14}NO) ligands. Additional splitting of each of these five HFS−components into additive five HFS components might be attributed to the interaction of the unpaired electron with four protons ($I = ½$) from two methylene groups adjacent to the sulfur atom in two cysteine ligands. The final 13-component HFS formed there upon explicitly suggests the presence of two cysteine ligands in this DNIC. After substitution of ^{14}NO for ^{15}NO in nitrosyl ligands with the nuclear spin of ^{15}N ($I = ½$), the interaction of the unpaired electron with two equivalent nitrosyl ligands yields only triplet HFS (Fig. 7b, *right* panel). Subsequent interaction of the unpaired electron with four protons from two methylene groups in two cysteine ligands gives a final nine-component HFS. In the absence of protons in the vicinity of thiol sulfur atoms in thiol-containing ligands (e.g., mercaptotriazole), the HFS is made up of five components formed as a result of interaction of the unpaired electron with two nitrosyl (^{14}NO) ligands (Fig. 7c, *right* panel). The EPR signal of this DNIC recorded at 77 K (Fig. 7c, *left* panel) differs essentially from the EPR signal characteristic of biological objects (especially, its central part). The latter shows complete coincidence only with the EPR signal of DNIC with cysteine and ^{14}NO ligands (Fig. 7a, *left* panel). And, finally, the doublet splitting in the EPR spectra of this model compound resulting from substitution of ^{56}Fe for ^{57}Fe ($I = ½$) unequivocally suggests the presence of only one iron atom in DNIC with cysteine (Fig. 7d, *right* panel).

All these data gave us substantial reason to hypothesize that paramagnetic DNIC with thiol-containing ligands responsible for the 2.03 signal in biological objects represent mononuclear dinitrosyl iron complexes (M-DNIC) with two thiol-containing (RS) ligands (their chemical formula appears as $[(RS)_2Fe(NO)_2]$) and that RS ligands in these DNIC are bound to positively charged iron ions (in the anionic form), i.e., to negatively charged sulfur atoms.

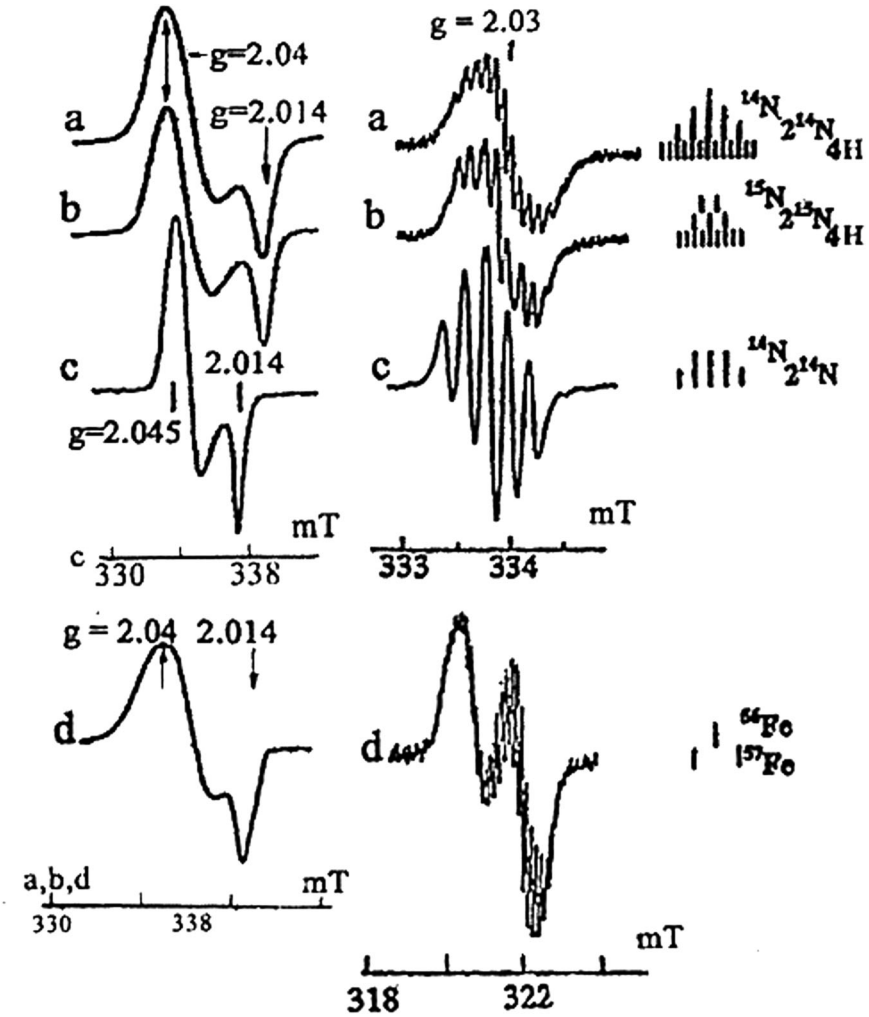

Fig. 7 The EPR spectra of DNIC-L-cysteine solutions containing ^{14}NO **a** or ^{15}NO **b**, DNIC with mercaptotriazole **c** and DNIC with cysteine containing ^{57}Fe **d** recorded at 77 K (*left*) or at ambient temperature (*right*) [15]

Similar conclusions were made in the aforecited paper by McDonald, Philips, and Mower [10] viz., in the absence of negatively charged (anionic) ligands DNIC pass from the mononuclear to the binuclear state characterized by the presence of thiol-containing ligands (B-DNIC, formula $(RS^-)_2Fe_2(NO)_4$), i.e., these complexes represent Roussin's red salt thioethers [15, 16].

This conversion is reversible, being determined by the chemical equilibrium between binuclear and mononuclear forms of B- and M-DNIC in accordance with Scheme 1: [14]

It is particularly M-DNIC with thiol-containing ligands that generate the 2.03 signal. B-DNIC represent diamagnetic, EPR-inactive complexes; their diamagnetism is conditioned by spin pairing of two iron-dinitrosyl ($Fe(NO)_2$) fragments of B-DNIC (the so-called "antiferromagnetic" interaction). If L-cysteine as a thiol-containing ligand is used at concentrations markedly exceeding the concentration of iron used in the synthesis of DNIC with cysteine at "physiological" pH, no <30% of iron binds to M-DNIC, while

$$2\ \text{M-DNIC} \underset{+RS^-}{\overset{-RS^-}{\Longleftrightarrow}} \text{B-DNIC}$$

Scheme 1 The interconversion of M- and B-DNIC with thiol-containing ligands

the remainder incorporates into B-DNIC. As regards M-DNIC with glutathione, no >10% of iron incorporates into these complexes at the same values of the glutathione: iron ratio and at "physiological" pH, i.e., in this case DNIC represent predominantly diamagnetic B-DNIC. With the increase in pH to 11.0–11.5, the concentration of M-DNIC with glutathione reaches ~100% of the total amount of DNIC due to transition of thiol groups of glutathione into the ionized (anionic) state [15, 17]. This transition is accompanied by considerable enhancement of the characteristic 2.03 signal of M-DNIC with thiol-containing ligands along with changes in the optical absorption spectra of the test solution manifested in the appearance of a single absorption band at 390 nm instead of two distinct optical

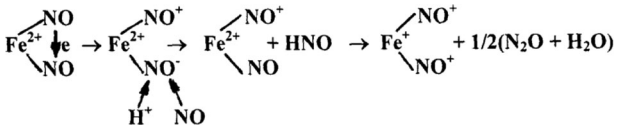

Scheme 2 The mechanism of $Fe(NO)_2$ fragment formation during the reaction of Fe(II) with neutral NO molecules

absorption bands at 310 and 360 nm characteristic of B-DNIC [15, 17, 18].

Studies by McDonald, Phillips, and Mower also demonstrated that DNIC with thiol-containing ligands can be easily generated upon mixing aqueous solutions of thiols and bivalent iron at neutral pH in the presence of gaseous NO [10]. A question arises: what is the mechanism whereby the interaction of two NO molecules with bivalent iron (both with the even total number of unpaired electrons, viz., two from NO and four from Fe^{2+}) yields paramagnetic iron-dinitrosyl fragments with the odd number of unpaired electrons? One of such hypothetical mechanisms is as follows (Scheme 2):[14, 19–22].

According to this Scheme, the nitroxyl ion generated in DNIC during the electron transfer from one NO molecule to the other as a result of disproportionation (mutual oxidation-reduction) of two NO molecules bound to bivalent iron, undergoes protonation and leaves the coordination sphere of iron in the form of the nitroxyl molecule. Subsequent disproportionation of nitroxyl molecules yields nitrous oxide (N_2O) and water. The vacant place in the coordination sphere of iron is immediately occupied by the other NO molecule resulting in the formation of paramagnetic iron-dinitrosyl fragments of DNIC with the d^7electronic configuration of iron and, as a consequence, the distribution of the electron spin density described by the formula $(Fe^{+}(NO^{+})_2$.

In aqueous solutions, nitrosonium ions (NO^+) undergo instantaneous hydrolysis. As result, $(Fe^{+}(NO^{+})_2$ fragments, which cannot exist in aqueous media, are expected to undergo rapid decomposition with the release of nitrite anions at neutral pH. However, depending on the nature of the thiol-containing ligands, these fragments can be preserved within the composition of DNIC for sufficiently long periods of time. Such stability of DNIC with thiol-containing ligands is determined by the transfer of the electron density from thiol sulfur atoms in DNIC characterized by high π-donor electronic activity to nitrosyl (NO^+) ligands able to accept it. As a result, the positive charge on nitrosyl ligands of DNIC diminishes, which strongly attenuates the interaction of these ligands with hydroxyl ions initiating the hydrolysis of NO^+ cations [22].

After establishing of the chemical equilibrium between M-DNIC with thiol-containing ligands and their constituent components when the ligands leave the coordination sphere

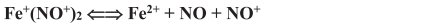

Scheme 3 The reversible equilibrium between $Fe(NO)_2$ fragments and their constituent components (Fe(II), NO, NO^+)

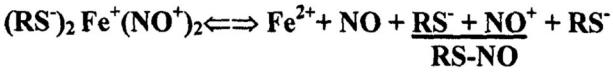

Scheme 4 The chemical equilibrium between M-DNIC and their constituent components (Fe(II), RS^-, NO, NO^+)

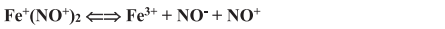

Scheme 5 The reversible equilibrium between $Fe(NO)_2$ fragments and their constituent components (Fe(III), NO^-, NO^+)

of iron, the chemical equilibrium for the iron-dinitrosyl fragments (the electron transfer from iron to NO^+) is described by Scheme 3 as: [17–22]

For M-DNIC, this transfer is described by Scheme 4: [14, 19–22]

A similar equilibrium seems to be characteristic of B-DNIC under the stipulation that the distribution of spin density in their two iron-dinitrosyl fragments is the same as that in the corresponding fragments of M-DNIC.

The ability of DNIC with thiol-containing ligands to donate neutral NO molecules and nitrosonium ions (NO^+) in living systems is easily explained in the paradigm of the hypothetical distribution of spin density in iron-dinitrosyl fragments. These complexes manifest high stability, which is further enhanced by the transfer of iron-dinitrosyl fragments from low-molecular DNIC to protein-bound thiol groups (cysteine residues) resulting in the formation of appropriate protein-bound M- and B-DNIC. The latter play the role of NO and NO^+ depots and are responsible for long-term persistence of DNIC in biological objects [19–22]. As regards the transfer of NO and NO^+ to their biological targets, this role is played by DNIC with low-molecular thiol-containing ligands [19, 20, 23]. It is the concentration of these ligands (for the most part, glutathione and cysteine) in body cells and tissues that determines the concentration of low-molecular DNIC and the efficiency of the transfer of NO and NO^+ to their biological targets. Under these conditions, neutral molecules of NO bind to heme-containing proteins, e.g., guanylatecyclase, while NO^+cations bind to thiol groups of proteins. In both cases, the transfer of NO and NO^+ to their biological targets is provided by higher (in comparison with iron) affinity of the latter for NO and NO^+ in DNIC.

In addition to the Scheme 3, two types of the chemical equilibrium can also exist for the transfer of two electrons from Fe^+ to NO^+ in iron-dinitrosyl fragments of DNIC (Schemes 5 and 6):

$$Fe^{+}(NO^{+})_2 \Longleftrightarrow Fe^{3+} + 2\ NO$$

Scheme 6 The reversible equilibrium between $Fe(NO)_2$ fragments and their constituent components (Fe(III), NO)

Under these conditions, DNIC with thiol-containing ligands act as NO, NO^{+}, and NO^{-}donors.

A comparison of HFS values for the splitting on the ^{57}Fe nucleus in M-DNIC, on nitrogen nuclei of nitrosyl ligands and on methylene group protons of cysteine ligands characteristic of EPR signals of DNIC with thiol-containing ligands at ambient temperature (Figs. 6 and 7) showed that the bulk of unpaired electronic density is localized on the d-orbital of iron or, more exactly, on the molecular orbital (MO) with the main contribution of the d-orbital of iron. Which of the five d-orbitals in M-DNIC is responsible for localization of the unpaired electron? The clue to this question can be found in the theoretical paper by B McGarvey [24] devoted to the calculation of the ratio between the values of the g-factor and the HFS tensor components for Co^{2+} nuclei [24]. This ratio is characteristic of the EPR signal of low-spin ($S = 1/2$) Co^{2+} complexes with phthalocyanins or porphyrins. These complexes have a d^7-electronic configuration of the central atom and the planar-square spatial characteristics also inherent in DNIC with thiol-containing ligands [24].

Our calculations of the values of the g-factor and HFS tensor components of ^{57}Fe in the EPR signals of M-DNIC with thiol-containing ligands (cysteine, glutathione, ethyl xanthogenate, and thiosulfate) showed that their g-factors were characterized by only two main values, viz., $g_{\perp}$and $g_{\parallel}$, suggesting that the paramagnetic centers have an axial spatial structure at $g_{\perp} > g_{\parallel} > 2.0023$ and $|A_{\perp}(^{57}Fe)| > |A_{\parallel}(^{57}Fe)|$[22]. For example, for the EPR signal of DNIC with cysteine these values were found to be identical, viz., $g_{\perp} = 2.04$, $g_{\parallel} = 2.014$ ($g_{aver.} = 2.03$) and $A_{\perp}(^{57}Fe) = -1.7$ mT, $A_{\parallel}(^{57}Fe) = -0.25$ mT, $A_{iso.} = -1.22$ mT. According to McGarvey et al. [24], such ratios between the values of the g-factor and the HFS tensor components for ^{57}Fe point to localization of the unpaired electron in DNIC on the d_{z^2} orbital of iron or, more specifically, on the molecular orbital (MO) with the main contribution of the d_{z^2} orbital of iron, viz., MO(d_{z^2}). It is of note that the localization of the unpaired electron on this orbital determines the formation of only one type of HFS, viz., anisotropic HFS. In its turn, the formation of isotropic HFS is determined by spin polarization of the electrons on the s-orbitals of iron due to localization of the unpaired electron on the d_{z^2} orbital of the iron atom [22].

This hypothesis is fully consistent with the diagram of the antibinding MO for DNIC with thiol-containing ligands characterized by low-spin d^7-electronic configuration of the iron atom, localization of the unpaired electron on the d_{z^2} orbital of iron and the planar-square spatial structure established in our laboratory as early as 1971 [25].

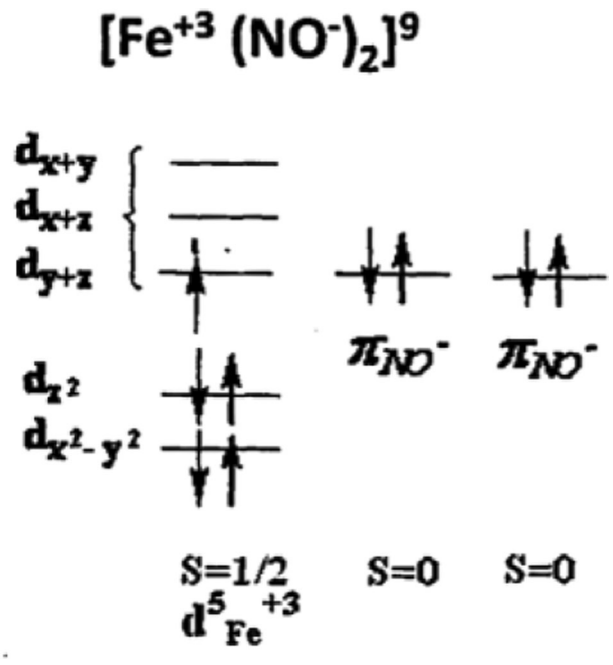

Scheme 7 Electron distribution on the d-orbitals of iron and the upper π-orbitals of nitrosyl ligands in $[Fe(NO)_2]^9$ fragment of M-DNIC with tetrahedral structure and d^5 electron configuration of iron

According to the Feltham-Enemark classification [26], which takes into account the total number of electrons on the d-orbitals of iron and the upper π-orbitals of the nitrosyl ligands in the Fe^{2+}-dinitrosyl fragments of DNIC, the electronic structure of DNIC with thiol-containing ligands is described by the formula $\{Fe(NO)_2\}^7$. However, many investigators hold the opinion that the total number of electrons on the d-orbitals of iron and the upper π-orbitals of nitrosyl ligands is nine instead of seven and that DNIC with nitrosyl ligands should, therefore, be classified as $\{Fe(NO)_2\}^9$ [27–30]. However, taking into consideration the spatial proximity of the π-orbitals of nitrosyl ligands to the d-orbitals of iron [31], the electronic structure of $Fe(NO)_2$ fragments can be finally presented as follows (Scheme7–9) [32]:

The hypothesis on the d^9 electronic configuration of the iron atom in DNIC with thiol-containing ligands based on the results of X-ray diffraction analysis suggests that in the crystal state the B-DNIC molecule has a tetrahedral structure where the iron atom is surrounded by four (two thiol and two nitrosyl) ligands. Judging from the distribution of energy between the d-orbitals in the tetrahedron (d_{xy},d_{yz}, d_{xz}) > ($d_{z2.}$ $d_{x^2-y^2}$), three out of seven electrons with the d^7 configuration of the iron atom are localized on the upper (d_x, $d_{yz,}$ and d_{xz}) orbitals. Moreover, according to the Hund rule, these electrons are arranged in parallel to one another in order to provide energy for high-spin DNIC at $S = 3/2$

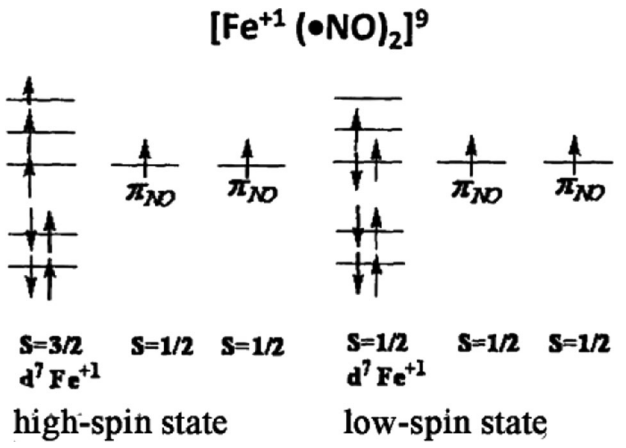

Scheme 8 Electron distribution on the d-orbitals of iron and the upper π-orbitals of nitrosyl ligands in $[Fe(NO)_2]^9$ fragment of M-DNIC with tetrahedral structure and d^7 electron configuration of iron

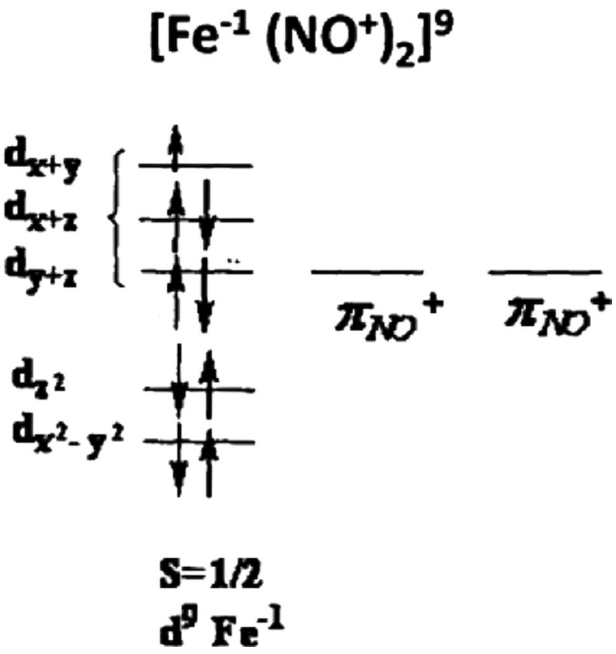

Scheme 9 Electron distribution on the d-orbitals of iron and the upper π-orbitals of nitrosyl ligands in $[Fe(NO)_2]^9$ fragment of M-DNIC with tetrahedral structure and d^9 electron configuration of iron

(Scheme 8). These DNIC are characterized by high spin-lattice relaxation; therefore, their EPR signals are detectable only at low temperatures. In actual fact, this is not the case, since EPR signals of these DNIC can just as well be measured at ambient temperature. To find a way out of this tricky situation, our worthy opponents supposed that the low-spin state of DNIC at $S = 1/2$ and the d^9 electronic configuration of the iron atom are due to the ability of upper d_{xy}, $d_{yz,}$ and d_{xz} orbitals to accept five (instead of three) electrons (Scheme 9). Similarly, their low-spin state ($S = ½$) can be attained if π-orbitals of nitrosyl ligands are able to accept at least four out of nine electrons (Scheme 7).

Needless to say, the reference to d-orbitals of iron without regard for molecular orbitals (MO) involving atomic orbitals of iron is a simplified approach to characterization of $Fe(NO)_2$ fragments, which is warranted only if the contribution of d-orbitals of iron to MO of $Fe(NO)_2$ fragments is taken into consideration.

A question arises to what extent the results of X-ray diffraction analysis of DNIC in the crystal state [27–30] are applicable to soluble DNIC present in biological objects. We are prone to think that dissolution of crystalline DNIC strongly affects their electronic and spatial characteristics as a result of which DNIC (or at least M-DNIC) acquire a planar-square structure and the electronic configuration proposed in ref. [25]. This structure offers a convenient paradigm for interpreting certain peculiarities of the EPR signal and some physico-chemical characteristics of M-DNIC. The views of our colleagues on this issue are diametrically opposite, viz., after dissolution DNIC fully preserve their tetrahedral structure and the d^9 electronic configuration of the iron atom, while the distribution of spin density within M-DNIC is described as $Fe^{-1}(NO^+)_2$.

What, then, are the pros and cons of our opponents' hypothesis? It is obvious that the increase in the electron density on the iron atom on going from the d^7 (Fe^{+1}) to the d^9 (Fe^{-1}) configuration can hardly influence the ability of DNIC to release NO or NO^+, since the latter is initially present in DNIC, while NO is generated during the transfer of electronic density from Fe^{-1} to NO^+. Our more recent findings suggest that the ratio between the values of the $g_\perp$ and $g_\parallel$ characteristic of the EPR signal of M-DNIC ($g_\perp > g_\parallel > 2.0$) can be also valid for M-DNIC with the tetrahedral structure and the d^9 electronic configuration of the iron atom. The difference between the values of $g_\perp$ and $g_\parallel$ for M-DNIC having the d^9 electronic configuration of the iron atom may result from the minor distortions in their tetrahedral structure and, as a consequence, from separation of MO (d_{xy}) from MO (d_{yz}) and MO (d_{xz}) and the subsequent transfer of the unpaired electron to MO (d_{xy}). Under these conditions, the energies of nine d-electrons will increase in the following order: MO (d_{z2}), MO ($d_{x^2-y^2}$) (four electrons) < MO (d_{yz}), MO (d_{xz}) (four electrons) < MO (d_{xy}) (1 electron). The values of the EPR signal, $g_\perp$ and $g_\parallel$, for this system of levels, which reflect their deviation from purely spin values, are determined by the transitions between MO (d_{xy}), MO (d_{yz}), and MO(d_{xz}) ($\Delta E_{(xy)-(xz,yz)}$) as well as between MO (d_{xy}) and MO ($d_{x^2-y^2}$) ($\Delta E_{(xy)-(x2-y2)}$). Since the value of the transition energy for MO (d_{xy}) on the one hand, and for MO (d_{yz}) and MO (d_{xz}), on the other hand, is appreciably smaller than for MO (d_{xy}) and MO ($d_{x^2-y^2}$), $g_\perp$ › $g_\parallel$ [22].

The applicability of the $|A_\perp(^{57}Fe)| > |A\|(^{57}Fe)|$ ratio to the EPR signals of M-DNIC with the d^9 electronic

configuration of the iron atom [24] and the ability of M-DNIC with thiol-containing ligands to accept two electrons [15, 18, 33] are still open to question and demand further verification and analysis. In the framework of the Enemark-Feltham $\{Fe(NO)_2\}^7$ classification, the acceptance of two electrons by M-DNIC with thiol-containing ligands is prerequisite to the transition of their iron-dinitrosyl fragments into the paramagnetic state $\{Fe(NO)_2\}^9$ characterized by the EPR signal with the following characteristics of the g-factor: $g_{\perp} = 2.01$, $g_{\parallel} = 1.97$, $g_{aver.} = 2.0$ [15, 18, 33]. Our analysis of the EPR spectra of two-electron reduction products of M-DNIC established that the accepted electrons were predominantly localized on the d-orbitals of iron as could be evidenced from the drastic (nearly threefold) increase in the width of the singlet EPR signal at $g = 2.0$ characteristic of doubly reduced M-DNIC with glutathione the ^{56}Fe atom in which was substituted for ^{57}Fe (Fig. 8b, d). Such broadening was related to the HFS of ^{57}Fe nuclei and was much more pronounced than that observed during the interaction of the unpaired electron with other magnetic nuclei, such as ^{14}N in nitrosyl ligands or protons in thiol-containing ligands. A similar effect was established during the analysis of the EPR signal generated by the product of two-electron reduction of B-DNIC with glutathione. In addition, at ambient temperature this compound produced a singlet EPR signal at $g = 2.0$ (Fig. 8e).

If additional electrons are indeed predominantly localized on the d-orbitals of iron (which is really the case judging from the characteristics of the EPR signal of ^{57}Fe-M-DNIC reduced by a two-electron mechanism (Fig. 8), the acceptance of the second electron by the iron atom in the original, d^9 configuration (Scheme 9) is impossible because of the inability of iron d-orbitals to accept more than ten electrons.

So, the use of only one approach, viz., EPR, allowed us not only to detect and to identify the paramagnetic centers responsible for the 2.03 signal of DNIC with thiol-containing ligands (predominantly, protein-bound ones) in biological objects, but also to establish their electronic and spatial structures responsible for their ability to act as NO and NO^+ donors.

More recent studies aimed at quantitative estimation of paramagnetic forms of DNIC with thiol-containing ligands (M-DNIC) in cultured cells carried out by a group of U.S. investigators established that DNIC synthesis is controlled by the weakly bound form of non-heme iron (the so-called labile iron pool). Under these conditions, the concentration of M-DNIC with thiol-containing ligands markedly exceeds the concentrations of other compounds whose synthesis is mediated by endogenous metabolites of NO, such as S-nitrosothiols and related nitroso- and nitro-compounds [34].

The first studies designed to investigate the role of the labile iron pool ("free" iron) in the synthesis of M-DNIC

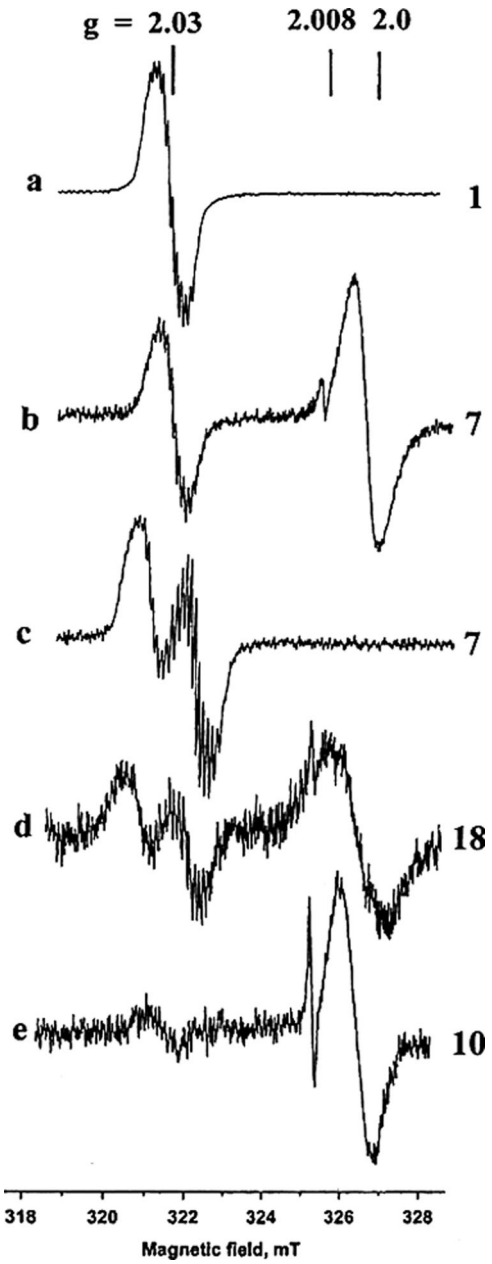

Fig. 8 The changes in the EPR spectra of 1 mM M-^{56}Fe-DNIC **a** and 1 mM M-^{57}Fe-DNIC (line **c**) with glutathione in 15 mM HEPES buffer (pH 7.4) induced by treatment of the complexes with sodium dithionite (**b** and **d**, respectively). **e** The changes in the EPR spectra of 1 mM B-^{56}Fe-DNIC with glutathione dissolved in 15 mM HEPES pH 7.4 induced by sodium dithionite treatment. All EPR spectra were recorded at ambient temperature [15]. The narrow EPR signal at $g = 2.008$ was generated by free-radical decomposition products of sodium dithionite

able to generate the 2.03 signal in animal tissues were carried out in our laboratory as early as the 1970's. In these studies, the dialysis of tissue samples was accompanied by elimination of "free" iron and a drastic decrease in the concentration of M-DNIC generated after treatment of

tissue extracts with gaseous NO or its water-soluble producers [35].

Our more recent EPR studies, established that in animal tissues the bulk of DNIC with thiol-containing ligands exists in the EPR-silent (diamagnetic) B-form of DNIC rather than in the EPR-active M-form. It was found also that the former is generated in large amounts in animal tissues in vivo in the presence of NO [36, 37].

These data were obtained in experiments where the dithiocarbamate derivative diethyldithiocarbamate (DETC) was used as acceptor of iron-mononitrosyl group. Its interaction with M- and B-DNIC with thiol-containing ligands (both low-molecular and protein-bound ones) and the further transfer of $Fe^{+}NO^{+}$ groups from iron-dinitrosyl fragments to thiocarbonyl groups of DETC gave paramagnetic MNIC with DETC (MNIC-DETC) (Fig. 9) [36, 37]. The use of this approach permitted us to detect diamagnetic (EPR-inactive) B-DNIC with thiol-containing ligands in animal tissues. As regards, the concentration of the paramagnetic form of DNIC (M-DNIC), it was established by the characteristic 2.03 signal of the EPR-active form in the absence of DETC. The EPR signals of MNIC-DETC containing ^{56}Fe or ^{57}Fe are shown in Fig. 10.

Our early studies aimed at establishing the spatial and electronic structures of MNIC-DETC were begun as early as the 1960's [38–43]. It was found that these complexes have a distorted square-pyramidal structure the two dithiocarbamate ligands in which are localized at the base of the pyramid, while the NO molecule occupies the axial position on its vertex. The unpaired electron is predominantly localized on the d_z^2 orbital of the iron atom [42]; therefore, the distribution of spin density in MNIC-DETC can be described as Fe^{+}-NO^{+}-(dithiocarbamate)$_2$. The electronic structure of MNIC with dithiocarbamate ligands thus appears to be identical to that of M-DNIC with thiol-containing ligands.

In 1984, we called the attention of practitioners in the field to the use of Fe^{2+}-DETC in animal studies in vivo as efficient spin traps of NO allowing subsequent EPR detection of MNIC-DETC [44]. The practical utility of this approach is in that the hydrophobic nature of Fe^{2+}-DETC, their specific localization and the ability to be accumulated in hydrophobic compartments of animal tissues prevent their release into circulating blood. The intensity of the EPR signal of MNIC-DETC enables monitoring the rate of NO accumulation in various body cells and tissues at definite periods of time. This approach has already won worldwide recognition among practitioners in the field: the number of publications devoted to their applications is steadily increasing with every passing year [45–48].

The high efficiency of this approach in determining NO concentration in animal tissues in vivo led us to hypothesize that in the absence of DETC NO bind to its endogenous

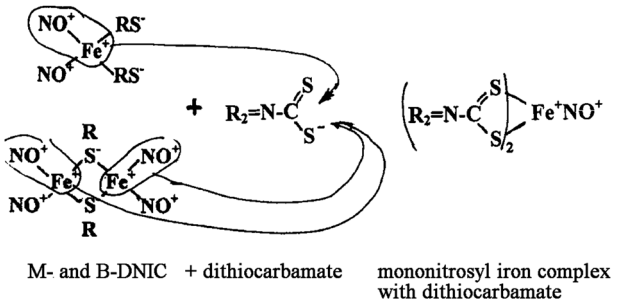

Fig. 9 The hypothetical mechanism of formation of paramagnetic MNIC-DETC by interaction of DETC with M- or B-DNIC with thiol-containing ligands [36]

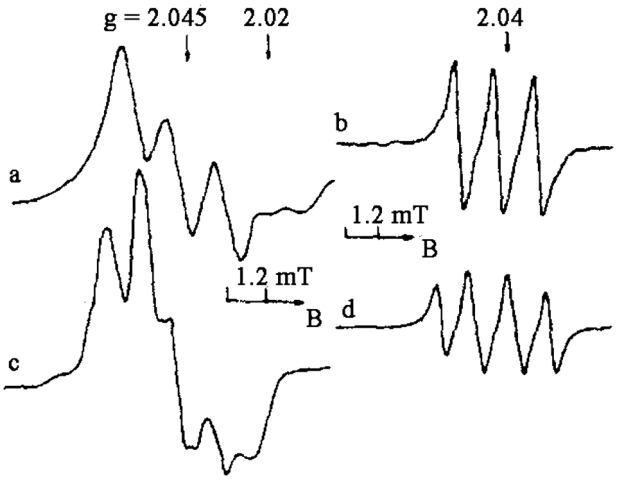

Fig. 10 The EPR signals of ^{56}Fe-MNIC-DETC **a**, **b**, and ^{57}Fe-MNIC-DETC **c**, **d** recorded at 77 K **a**, **c** or at ambient temperature **b**, **d** [38]

traps, in the first place, to free iron and thiol-containing compounds to give endogenous DNIC with thiol-containing ligands [36, 37]. As stated above, the mononuclear form of these DNIC was easily detectable by the characteristic 2.03 signal. As regards EPR-inactive B-DNIC, they might be converted into paramagnetic MNIC-DETC by simple treatment with DETC even in experiments with isolated tissues in vitro. Therefore, the concentration of original B-DNIC was determined by the characteristic EPR signal of MNIC-DETC.

The totality of our experimental data provides conclusive evidence in favor of this hypothesis [36, 37]. A distinct 2.03 signal of protein-bound M-DNIC was found in the EPR spectra of isolated mouse livers after 30-min intraperitoneal treatment of animals with B-DNIC with glutathione (0.5 ml of 5 mM DNIC); its intensity did not change after perfusion of liver tissues with 15 mM HEPES pH 7.4 (Fig. 11a). However, after perfusion of tissue samples with the same solution at pH 13.0, the EPR signal increased by ~30% (Fig. 11b), most probably at the expense of thiol groups ionized at the sulfur atom, which initiated

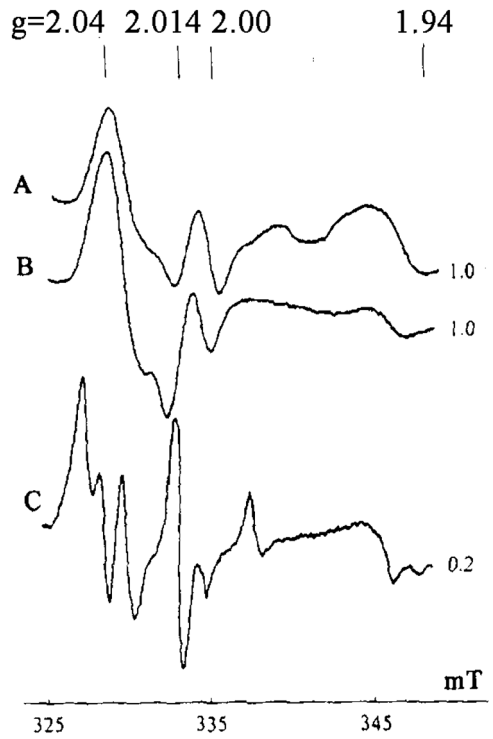

Fig. 11 The EPR spectra recorded in mouse liver 30-min after i/p treatment of animals with B-DNIC with glutathione and subsequent perfusion of isolated livers with 15 mM HEPES pH 7.4 **a**, pH 13.0 **b** and pH 7.4 + 200 mM DETC **c**. All EPR spectra were recorded at 77 K. The figures on the *right* indicate amplification of the radiospectrometer (in arb. units). The EPR signals recorded at $g = 2.04$ and 2.014, 2.0, and 1.94 were generated by M-DNIC with thiol-containing ligands, free radicals and reduced iron-sulfur proteins, respectively [36]

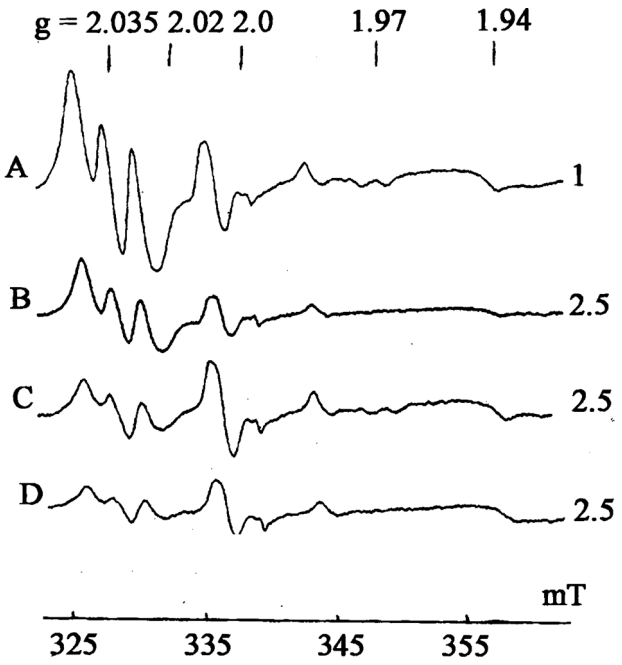

Fig. 12 The EPR spectra recorded in the livers of mice treated with LPS for 4 h followed by 30-min infusion of DETC + Fe^{2+} **a** or pure iron (Fe^{2+}) and in vitro perfusion of liver tissues with DETC **b** or pure DETC **c**. **d** The EPR spectra recorded in isolated liver tissues of mice treated with LPS (4 h) and perfused with DETC in vitro. All EPR spectra were recorded at 77 K. The figures on the *right* designate the amplification of the radiospectrometer (in arb. units). The EPR signals recorded at $g = 2.035$ and 2.02 were generated by MNIC-DETC; those recorded at $g = 2.0$, 1.97, and 1.94 were produced by endogenous free radicals, molybdenum complexes, and reduced iron-sulfur proteins, respectively [36]

partial conversion of B-DNIC into paramagnetic M-DNIC (Scheme 1).

The EPR spectra recorded after perfusion of mouse livers with 200 mM DETC in 15 mM HEPES pH 7.4 contained an EPR signal of MNIC-DETC with triplet HFS instead of the 2.03 signal (Fig. 11c). Judging from its intensity, the concentration of MNIC-DETC exceeded that of the original complexes more than fivefold, which might be attributed to the conversion of B-DNIC into MNIC-DETC by the mechanism depicted in Fig. 9.

It would appear natural if both protein-bound B-DNIC and added low-molecular B-DNIC with glutathione were involved in this process. With this in mind, in the next series of our experiments we set ourselves the task to investigate the ability of DETC to detect B-DNIC with thiol-containing ligands in animal tissues. In one of these studies, treatment of mice with bacterial lipopolysaccharide (LPS) for 4 h initiated the synthesis of inducible forms of NO synthase (iNOS), resulting in enhanced production of NO in animal tissues. Judging from the EPR signal, the concentration of MNIC-DETC in mouse liver amounted to 90±30 μmoles per kg wet liver mass (as calculated per one iron atom in MNIC-DETC) (Fig. 12a). To detect NO, the animals underwent 30-min treatment with DETC (500 mg/kg of body mass) and the Fe^{2+} complex (50 mg of $FeSO_4$ per kg of body mass) with citrate (250 mg/kg body mass). After treatment with DETC alone, the concentration of MNIC-DETC in mouse liver remained at a level of 18±7 μmoles per kg wet liver mass (as calculated per one iron atom in MNIC-DETC) as could be evidenced from the intensity of their EPR signal (Fig. 12c).

MNIC-DETC were also found in the livers of LPS-treated mice 30 min after administration of Fe^{2+} + citrate or DETC. After killing of mice, liver tissues were extracted and perfused in vitro with 200 mM DETC. Judging from the intensity of the EPR signals (Fig. 12b, d), the concentration of MNIC-DETC varied from 18±4 to 8±3 μmoles per kg of wet tissue (as calculated per one atom iron in MNIC-DETC). The lack, in the EPR spectra of LPS-treated mice, of the characteristic 2.03 signal of M-DNIC with thiol-containing ligands led us to conjecture that in liver tissues of DETC-treated mice MNIC-DETC were formed during the interaction of DETC with B-DNIC in the presence of endogenous NO whose synthesis was initiated by inducible

NOS. The concentration of MNIC-DETC was supposed to increase after treatment of animals with Fe^{2+}.

Considering that the formation of one Fe^{2+}-dinitrosyl [$Fe(NO)_2$] fragment of B-DNIC requires three molecules of NO (Scheme 2), the concentration of MNIC–DETC (~18 μmoles/kg) formed in liver tissues of mice after treatment with LPS and Fe^{2+} and subsequent treatment of tissue samples with DETC must correspond to 54 μmoles/kg of NO formed in the liver by iNOS and included into B-DNIC. This concentration constitutes 60% of the whole amount of NO in MNIC–DETC (90 μmoles/kg) generated in liver tissues as a result of binding of NO to Fe-DETC in vivo. Presumably, the rest (40%) of MNIC-DETC are produced by S-nitrosothiols able to generate MNIC-DETC during their interaction with Fe-DETC [38].

Conclusive Remarks

The totality of the experimental data unequivocally suggest that the EPR method is an adequate and all-sufficient procedure for detecting and identifying paramagnetic (mononuclear) and diamagnetic (binuclear) forms of DNIC with thiol-containing ligands (M- and B-DNIC, respectively) in animal and bacterial cells and tissues. The full identity of the major characteristics of the 2.03 signal recorded in living systems to those of the EPR signal recorded in frozen solutions of low-molecular (model) DNIC with thiol-containing ligands established in our laboratory as early as the 1960's was a crucial factor in the discovery and identification of M-DNIC (so-called 2.03 complexes) [7, 11]. Moreover, it allowed a conclusion that in living systems 2.03 complexes are represented by M-DNIC with low-molecular or protein-bound thiol-containing ligands. Our EPR analysis of various characteristics of model M-DNIC shed additional light on the electronic structure of 2.03 complexes responsible for their biological activity as NO and NO^+ donors. As regards B-DNIC with thiol-containing ligands, their recent discovery in animal tissues by the EPR method [36] was determined by their ability to be converted into EPR-detectable MNIC-DETC after treatment with DETC.

The ability of DNIC with thiol-containing ligands to act as NO donors (Schemes 3 and 4) was confirmed by the results of chemical and biological studies [17–23, 32–37]. As regards their ability to generate S-nitrosothiols (RS-NO) by Scheme 4, it demands more investigation and analysis. The generation of RS-NO easily detectable in acid solutions by optical methods during decomposition of DNIC failed to be established in aqueous media at neutral pH [17]. It is not improbable that the formation of nitrite anions instead of RS-NO in the course of hydrolysis is related to the inability of thiols (e.g., glutathione) to compete with hydroxyl ions for nitrosonium ions released from DNIC (Scheme 4). After acidification of the medium, which diminishes the concentration of hydroxyl ions by several orders of magnitude, the competitive activity of thiols increases as a result of their interaction with nitrosonium ions culminating in the appearance of RS-NO.

The ability of DNIC with thiol-containing ligands to initiate the formation of RS-NO in animal cells in vivo was established in earlier studies [49, 50]. The mechanism responsible for the predominance of thiols over hydroxyl anions during the interaction of the former with NO^+ is still unclear and demands further verification and analysis. It is not excluded that in living systems this interaction is determined by the specific characteristics of thiols and the composition of the reaction medium. Special mention should be made of the recently established ability of *N*-methyl-D-glucaminedithiocarbamate (MGD) to produce simultaneously MNIC-MGD and the corresponding S-nitrosothiol during the interaction of the former with B-DNIC with glutathione [17]. One should not rule out the possibility that this phenomenon can be due to the higher (in comparison with hydroxyl anions) affinity of thiol groups of MGD for NO^+.

The high biological activity of M- and B-DNIC with thiol-containing ligands as donors of NO, one of the most universal regulators of biological processes [18–21, 27], and their wide occurrence in living systems [27, 36] strongly suggest that these complexes have every reason to be regarded as a "working form" of NO [27].

Acknowledgements This work has been carried out with the financial support of the Russian Foundation of Basic Research (Grant No. 15-04-00708-a) and the Russian Scientific Foundation (Grant No. 16-13-10295)

Compliance with ethical standards

Conflict of interest The author declares that they have no competing interests.

References

1. Nalbandyan, R. M., Vanin, A. F., & Blumenfeld, L. A. (1964) Free radicals in yeast cells. Abstracts of the Meeting "Free Radicals Processes in Biological Systems", Moscow, p. 18.
2. Vanin, A. F., & Nalbandyan, R. M. (1965). Free radicals of a new type in yeast cells. *Biofizika (Rus)*, *10*, 167–168.
3. Lebedev, J. S. (1963). Computer calculations of EPR spectra.2. Asymmetric lines. *Zhurnal Strukt. Khimii (Rus)*, *4*, 1074–1078.
4. Vanin, A. F., & Nalbandyan, R. M. (1966). Free radical species with unpaired electron localization on sulfur atom in yeast cells. *Biofizika (Rus)*, *11*, 178–179.
5. Vithaythil, A. J., Ternberg, B., & Commoner, B. (1965). Electron spin resonance signals of rat liver during chemical carcinogenesis. *Nature*, *207*, 1246–1249.

6. Mallard, J. R., & Kent, M. (1964). Difference observed between electron spin resonance signals from surviving tumour tissues and from their corresponding normal tissues. *Nature*, *204*, 1192.
7. Vanin, A. F., Blumenfeld, L. A., & Chetverikov, A. G. (1967). Investigation of non-heme iron complexes in cells and tissues by the EPR method. *Biofizika (Rus)*, *12*, 829–841.
8. Lancaster, J. R., & Hibbs, J. B. (1990). EPR demonstration of iron-nitrosyl complex formation by cytotoxic activated macrophages. *Proceedings of the National Academy of Sciences USA*, *87*, 1223–1227.
9. Woolum, J. C., & Commoner, B. (1970). Isolation and identification of a paramagnetic complex from livers of carcinogen-treated rats. *Biochimica et Biophysica Acta*, *201*, 131–140.
10. McDonald, C. C., Philips, W. D., & Mower, H. F. (1965). An electron spin resonance study of some complexes or iron, nitric oxide and anionic ligands. *Journal of the American Chemical Society*, *87*, 3319–3326.
11. Vanin, A. F. (1967). Identification of divalent iron complexes with cysteine by the EPR method. *Biokhimia (Rus)*, *32*, 228–232.
12. Vanin, A. F., Kubrina, L. N., Lisovskaya, I. L., Malenkova, I. V., & Chetverikov, A. G. (1971). Endogenous heme and nonheme nitrosyl iron complexes in cells and tissues. *Biofizika (Rus)*, *16*, 650–658.
13. Vanin, A. F., Kiladze, S. V., & Kubrina, L. N. (1977). Factors influencing the formation of the dinitrosyl complexes of non-heme iron in animal organs in vivo. *Biofizika (Rus)*, *22*, 850–857.
14. Vanin, A. F. (1980) Nitrosyl non-heme iron complexes in animal tissues and microorganisms. Doctoral Thesis, Institute of Chemical Physics, Moscow.
15. Vanin, A. F., Poltorakov, A. P., Mikoyan, V. D., Kubrina, L. N., & Burbaev, D. S. (2010). Polynuclear water-soluble dinitrosyl iron complexes with cysteine or glutathione ligands: electron paramagnetic resonance and optical studies. *Nitric Oxide Biology and Chemistry*, *23*, 1236–1249.
16. Wang, R., Camancho-Fernandez, M. A., Xu, W., Zhang, J., & Li, L. (2009). Neutral and reduced Roussin's red salt ether [Fe^2 $(\mu\text{-RS})_2$ $(NO)_4$] (R= n-Pr, t-Bu, 6-methyl-2-pyridyl and 4,6-dimethyl-2-pyrimidyl): synthesis, X-ray crystal structure, spectroscopic, electrochemical and density functional theoretical investigations. *Dalton Transactions*, *5*, 777–786.
17. Borodulin, R., Kubrina, L. N., Mikoyan, V. D., Poltorakov, A. P., Shvydkiy, V. O., Burbaev, D. S., Serezhenkov, V. A., & Vanin, A. F. (2013). Dinitrosyl iron complexes with glutathione as NO and NO^+ donors. *Nitric Oxide Biology and Chemistry*, *29*, 4–16.
18. Borodulin, R., Kubrina, L. N., Serezhenkov, V. A., Burbaev, D. S. h., Mikoyan, V. D., & Vanin, A. F. (2013) Redox conversion of dinitrosyl iron complexes with natural thiol-containing ligands, *35*, 35–41.
19. Vanin, A. F. (2009). Dinitrosyl iron complexes with thiolate ligands: Physico-chemistry, biochemistry and physiology. *Nitric Oxide Biology and Chemistry*, *21*, 1–13.
20. Vanin, A. F. (2015) Dinitrosyl iron complexes with natural thiol-containing ligands: Physicochemistry, Biology, and Medicine. In G. Jaouen & M. Salmain (Eds), *Bioorganometallic chemistry, applications to drug discovery, biocatalysis and imaging* (pp. 203–238). Wiley-VCH Verlag GmbH.
21. Vanin, A. F., & van Faassen, E. (2007). DNICs: physico-chemical properties and their observation in cells and tissues. In E. van Faassen & A. F. Vanin (Eds), *Radicals for life: The various forms of nitric oxide* (pp. 19–73). Amsterdam: Elsevier.
22. Vanin, A. F., & Burbaev, D. S. (2011). Electronic and spatial structures of water-soluble dinitrosyl iron complexes with thiol-containing ligands underlying their activity to act as nitric oxide and nitrosonium ion donors. *Biophysical Journal*, *14*, 878236.
23. Timoshin, A. A., Lakomkin, V. L., Abramov, A. A., Ruuge, E. K., Kapel'ko, V. I., Chazov, E. I., & Vanin, A. F. (2015). The hypotensive effect of the nitric monoxide donor Oxacom at different routes of its administration to experimental animals. *European Journal of Pharmacology*, *765*, 525–532.
24. McGarvey, B. R. (1975). Theory of the spin Hamiltonian parameters for low spin cobalt (II) complexes. *Canadian Journal of Chemistry*, *53*, 2498–2511.
25. Burbaev, D. S., Vanin, A. F., & Blumenfeld, L. A. (1971). Electronic and spatial structures of paramagnetic dinitrosyl ferrous complexes. *Zhurnal Strukt. Khimii (Rus)*, *12*, 252–256.
26. Enemark, J. H., & Feltham, R. D. (1974). Principles of structure, bonding, and reactivity for metal nitrosyl. *Coordination Chemistry Reviews*, *13*, 339–406.
27. Tsou, C. C., Lu, T. T., & Liaw, W. F. (2007). EPR, UV-vis and X-ray demonstration of the anionic dimeric dinitrosyl iron complexes $[(NO)_2Fe(SBut)_2(NO)_2]$: relevance to the product of nitrosylation of cytosolic and mitochondrial aconitases, and high-potential iron proteins. *Journal of the American Chemical Society*, *129*, 12626–12627.
28. Lu, T. T., Tsou, C. C., Huang, H. W., Hsu, I. J., Chen, J. M., Kuo, T. S., Wang, Y., & Liaw, W. F. (2008). Anionic Roussin's Red Ethers (RREs)syn-lanti-$[Fe\text{-}SE'(NO)_2]_2$: the critical role of thiolate ligands in regulating the transformation of RREs into dinitrosyl iron complexes and the anionic RREs. *Inorganic Chemistry*, *47*, 6040–6050.
29. Tinberg, C. E., Tonzetich, Z. J., Wang, H., Do, L. H., Yoda, Y., Cramer, S. P., & Lippard, S. J. (2010). Characterization of iron dinitrosyl species formed in the reaction of nitric oxide with a biological Rieske center. *Journal of the American Chemical Society*, *132*, 18168–18176.
30. Shestakov, A. F., Shul'ga, Yu. M., Emel'yanova, N. S., Sanina, N. A., & Aldoshin, S. M. (2007). Molecular and electronic structure and IR spectra of mononuclear dinitrosyl iron complex $[FeSC_2H_3N_3)$ $(Sc_2H_3N_3)]$: a theoretical study. *Russian Chemical Bulletin*, *56*, 1289–1297.
31. Reginato, N., Mc Crory, C. T. C., Pervitsky, D., & Li, L. (1999). Synthesis, X-ray crystal structure and solution behavior of $Fe(NO)_2$(1-Melm)2: Implications for nitrosyl non-heme iron complexes with g=2.03. *Journal of the American Chemical Society*, *121*, 10217–10218.
32. Aldoshin, S. M., Sanina, N. A., Davydov, M. I., & Chazov, E. I. (2016). New class of NO donors. *Herald of the Russian Academy of Sciences*, *86*, 158–163.
33. Borodulin, R. R., Dereven'kov, I. A., Makarov, S. V., Mikoyan, V. D., Serezhenkov, V. A., Kubrina, L. N., Ivanovich-Burmazovich, I., & Vanin, A. F. (2014). Redox activities of mono- and protein-bound dinitrosyl iron complexes with thiol-containing ligands. *Nitric Oxide Biology and Chemistry*, *40*, 100–109.
34. Hickok, J. R., Sahni, S., Shen, H., Arvindt, A., Antoniou, C., Fung, L. M. W., & Thomas, D. D. (2011). Dinitrosyl iron complexes are the most abundant nitric oxide-derived cellular adducts: biological parameters of assembly and disapearance. *Free Radical Biology and Medicine*, *51*, 1558–1566.
35. Vanin, A. F., Osipov, A. N., Kubrina, L. N., Burbaev, D. Sh, & Nalbandyan, R. M. (1975). On the origin of paramagnetic centers with g=2.03 in animal tissues and microorganisms. *Studia Biophysica*, *49*, 13–25.
36. Vanin, A. F., Mikoyan, V. D., Kubrina, L. N., Borodulin, R. R., & Burgova, E. N. (2015). Mono- and binuclear dinitrosyl iron complexes with thiol-containing ligands in various biosystems. *Biofizika (Rus)*, *60*, 735–747.
37. Vanin, A. F. (2016). Dinitrosyl iron complexes with thiol-containing ligands as a "working form" of endogenous nitric oxide. *Nitric Oxide Biology and Chemistry*, *54*, 15–29.

38. Vanin, A. F. (1999). Iron diethyldithiocarbamate as spin trap for nitric oxide detection. *Methods in Enzymology*, *301*, 269–278.
39. Gibson, J. (1962). Unpaired electron in nitroso-bis-(dimethyldithiocarbamate) iron(II). *Nature*, *196*, 64.
40. Gray, H. B., Bernal, I., & Billig, E. (1962). The electronic structure of metal nitrosyls and carbonyls. *Journal of the American Chemical Society*, *84*, 3404–3405.
41. Colapietro, M., Domenicano, A., Scaramuzza, I., Vaciago, A., & Zambomelli, L. (1967) The crystal and molecular structure of nitrosyliron bis-(N,N-diethyldithiocarbamate). *Chemical Communications* 583–584.
42. Frank, E., & Abeledo, C. R. (1969). Messbauer effect in nitrosyl iron(II) bis-dithiocarbamate. *Journal of Inorganic and Nuclear Chemistry*, *31*, 989–993.
43. Goodman, B.A., Raynor, J.B., & Symons, M.C.R. (1969) Electron spin resonance of bis-(NN-diethyldithiocarbamate)nitrosyliron. *Journal of Chemical Society (A)*, 2572–2575.
44. Vanin, A. F., Mordvintcev, P. I., & Kleschyov, A. L. (1984). Appearance of nitric oxide in animal tissues in vivo. *Studia Biophysica*, *102*, 135–143.
45. Kleschyov, A., Mollnau, H., Oelze, M., Meinertz, T., Huang, Y., Harrison, D., & Munzel, T. (2000). Spin trapping of vascular nitric oxide using colloid Fe(II)-diethyldithiocarbamate. *Biochemical and Biophysical Research Communications*, *275*, 672–767.
46. Nagano, T., & Yoshimura, T. (2002). Bioimaging of nitric oxide. *Chemical Reviews*, *102*, 1235–1269.
47. Yoshimura, T., & Kotake, Y. (2004). Spin trapping of nitric oxide with the iron-dithiocarbamate complex: chemistry and biology. *Antioxidants & Redox Signaling*, *5*, 639–647.
48. Vanin, A. F., & Timoshin, A. A. (2011). Determination of in vivo nitric oxide levels in animal tissues using a novel spin trapping technology. *Methods in Molecular Biology*, *704*, 135–149.
49. Bosworth, C. A., Toledo, J. C., Zmijewski, J. W., Li, Q., & Lancaster, J. R. (2009). Dinitrosyliron complexes and the mechanism(s) of cellular protein nitrosothiol formation from nitric oxide. *Proceedings of the National Academy of Sciences USA*, *106*, 4671–4676.
50. Foster, M. W., Liu, L., Zeng, M., & Stamler, J. S. (2009). A genetic analysis of nitrosative stress. *Biochemistry*, *48*, 792–799.